Journal of Power Sources 256 (2014) 1–7

Contents lists available at ScienceDirect

Journal of Power Sources

journal homepage: www.elsevier.com/locate/jpowsour

Improved cycle stability and high-rate capability of Li_3VO_4-coated Li[$Ni_{0.5}Co_{0.2}Mn_{0.3}$]O_2 cathode material under different voltages

Yan Huang, Feng-Min Jin, Fang-Jie Chen, Li Chen*

Department of Chemistry, Tianjin University, Tianjin 300072, People's Republic of China

HIGHLIGHTS

- Electrochemical performance of Li[$Ni_{0.5}Co_{0.2}Mn_{0.3}$]O_2 is improved by Li_3VO_4 coating.
- Li[$Ni_{0.5}Co_{0.2}Mn_{0.3}$]O_2 coated with 3 wt.% Li_3VO_4 shows the best high-rate capability.
- Cycle stability of Li_3VO_4-coated Li[$Ni_{0.5}Co_{0.2}Mn_{0.3}$]O_2 at 10 C is obviously improved.
- Li_3VO_4-coated Li[$Ni_{0.5}Co_{0.2}Mn_{0.3}$]O_2 shows better high voltage cycliability (4.8 V).

ARTICLE INFO

Article history:
Received 24 October 2013
Received in revised form
11 December 2013
Accepted 1 January 2014
Available online 9 January 2014

Keywords:
Lithium vanadate-coated
High-rate performance
Cycle stability
High voltage

ABSTRACT

Li_3VO_4-coated Li[$Ni_{0.5}Co_{0.2}Mn_{0.3}$]O_2 cathode material exhibits much better cycling stability, rate capability, and high voltage cycling behavior than pristine Li[$Ni_{0.5}Co_{0.2}Mn_{0.3}$]O_2 at room temperature. The sample coated with 3 wt.% Li_3VO_4 shows the optimum electrochemical performance. It delivers a capacity of 61.5 mAh g^{-1} at 10 C (1800 mA g^{-1}) after 100 cycles. The capacity retention at 1 C (180 mA g^{-1}) is 63.5% at cut-off voltage 4.6 V, and 63.0% at a higher cut-off voltage 4.8 V. XRD and XPS results reveal that the Li_3VO_4 coating layer reinforces the surface of matrix material, which benefits structural stability of Li[$Ni_{0.5}Co_{0.2}Mn_{0.3}$]O_2 during long-term cycling. CV and EIS tests indicate that the improvement of electrochemical performances could be attributed to higher Li^+ conductivity, suppression of Co and Mn dissolution from Li[$Ni_{0.5}Co_{0.2}Mn_{0.3}$]O_2, and decreased polarization during cycling since Li_3VO_4 layer on Li[$Ni_{0.5}Co_{0.2}Mn_{0.3}$]O_2 surface acts as a relatively stable protective barrier as well as an excellent Li-ion conductor.

1. Introduction

Li[$Ni_{1-x-y}Co_xMn_y$]O_2 [1,2], as a derivative of $LiNiO_2$, is considered to be one of the most promising substitutes for $LiCoO_2$ because of the cost and unsafety of $LiCoO_2$ [3]. Among them, the classical Li[$Ni_{1/3}Co_{1/3}Mn_{1/3}$]O_2 [4] has been successfully applied to Li-ion batteries. Nevertheless, its low rate capability, poor thermal stability and large capacity loss [4,5] at high cut-off voltage still need to be improved to meet the requirement of high-power and high-capacity for hybrid electric vehicles.

Li[$Ni_{0.5}Co_{0.2}Mn_{0.3}$]O_2 [6] is regarded as another potential cathode material for industrial application. With high Ni content, it shows high reversible capacity and wide operating voltage range (2.8–4.8 V), but poor cycle stability and rate capability, which originate from structure disruption and cation-mixing between Li^+ and Ni^{2+} during cycling [7], need to be improved.

Doping is an effective method to improve electrochemical properties of cathode materials. Slight dopant ions, such as Al^{3+} [8], Mg^{2+} [9], Zr^{4+} [10], and Zn^{2+} [11], can stabilize crystal structure, but have to sacrifice some capacity due to the addition of electrochemically inactive elements [8].

Surface modification is another effective way to enhance electrochemical properties of materials. Kim et al. [5] have reported that Li[$Ni_{0.5}Co_{0.2}Mn_{0.3}$]O_2 with a $LiFePO_4$ coating layer showed stable discharge behaviors at high rates and elevated thermal stability. Liu et al. [12] have proven that Li[$Ni_{1/3}Co_{1/3}Mn_{1/3}$]O_2 with a V_2O_5 coating layer could enhance the cycliability and rate capability of electrodes. Pu et al. [13] have suggested that $LiCoO_2$ with a Li_3VO_4 coating layer exhibited a good cycliability and high-rate capability at lower discharge rate 0.2 C.

2. Experimental

Li[$Ni_{0.5}Co_{0.2}Mn_{0.3}$]O_2 was prepared by calcining a stoichiometric mixture of [$Ni_{0.5}Co_{0.2}Mn_{0.3}$]$(OH)_2$ precursor and $LiOH\cdot H_2O$ at

* Corresponding author. Tel.: +86 22 27892379; fax: +86 22 27403475.
E-mail address: chenli_su@eyou.com (L. Chen).

0378-7753/$ – see front matter © 2014 Published by Elsevier B.V.
http://dx.doi.org/10.1016/j.jpowsour.2014.01.003

500 °C for 5 h, then at 900 °C for 24 h, subsequently was coated with Li_3VO_4 by a wet chemical process. A solution was obtained by successively dissolving LiOH and V_2O_5 (at a 6:1 M ratio) in deionized water, then $Li[Ni_{0.5}Co_{0.2}Mn_{0.3}]O_2$ powders were added into the above solution under vigorous stirring. After evaporating solvent at 80 °C for 3 h, the obtained powders were sintered at 700 °C for 8 h to get coated $Li[Ni_{0.5}Co_{0.2}Mn_{0.3}]O_2$ materials with 1, 2, 3, and 4 wt.% Li_3VO_4, which were, respectively, denoted as sample 1, 2, 3, 4, and the uncoated $Li[Ni_{0.5}Co_{0.2}Mn_{0.3}]O_2$ powders was denoted as sample 0.

The crystalline phase of the prepared samples were studied by Powder X-ray diffraction (XRD, D/max 2500 V/PC, Rigaku, 40 kV, 150 mA) using Cu Kα radiation ($\lambda = 1.5405$ Å) and a bent graphite monochromatic with a scan speed of 2° min^{-1} in the 2θ range 10–90°. The microstructure characterization of the sample was analyzed using transmission electron microscope (TEM, JEM-2100F, JEOL) with a energy-dispersive spectroscopy (EDS) at an accelerating voltage of 200 kV. Surface chemical composition and binding energy were analyzed by X-ray photoelectron spectroscopic (XPS, AXIS Ultra DLD, Kratos) employing a Al Kα (1486.6 eV) excitation source. All XPS spectra were recorded using an aperture slot of 300 × 700 microns. Survey spectra were recorded with a pass energy of 160 eV and high resolution spectra with a pass energy of 40 eV. Vacuum in the test chamber was 1×10^{-9} Torr. The binding energy was corrected by taking C1s (284.6 eV) as a criterion.

The slurry was prepared by mixing active materials with carbon black and PVDF (polyvinylidene fluoride) in a weight ratio of 8:1:1, subsequently it was cast onto Al foil, and dried at 120 °C under vacuum for 12 h. The dried plate was punched into round disk with a diameter of 1.2 cm and subsequently rolled into a thin film with a thickness of 32 μm. The coin cell was then assembled in argon glove box, with lithium metal as the anode and 1 M $LiPF_6$ in EC: DEC: EMC (1:1:1 by volume) as the electrolyte. The electrochemical property was investigated using a constant current/constant voltage (CC/CV) method for charging and a CC method for discharging at different rate. Cyclic voltammetry (CV) tests were performed using an electrochemical workstation (CHI 660D) between 2.5 and 4.9 V vs. Li/Li^+ at a scan rate of 0.05 mV s^{-1}. Electrochemical impedance spectroscopy (EIS) measurements were carried out with an electrochemical workstation PARSTAT 2273 in the frequency range from 10 mHz to 100 kHz.

3. Results and discussion

The initial charge–discharge curves of all samples, in the voltage range of 2.8–4.6 V and at 0.1 C (18 mA g^{-1}), are given in Fig. 1. In contrast to sample 0, all coated samples exhibit a lower charge voltage plateau and a higher long discharge voltage plateau, which leads to their higher discharge capacities. Moreover, the charge-discharge voltage plateaus (corresponds to Ni^{2+}/Ni^{4+} redox couple [14]) of all coated samples are closer to 3.7 V than that of sample 0, which indicates that Li_3VO_4 surface coating improves the reversibility of electrode reaction by reducing electrode polarization. No new plateau is observed in coated samples, which indirectly proves that Li_3VO_4 is not involved in the electrode reaction.

The cycle performances of all samples are shown in Fig. 2. The cells were cycled at 10 C in the voltage range of 2.8–4.6 V. The discharge capacities of sample 0, 1, 2, 3, 4, are respectively 2.5 mAh g^{-1}, 44.5 mAh g^{-1}, 48.1 mAh g^{-1}, 61.5 mAh g^{-1}, and 53.5 mAh g^{-1} after 100 cycles, and the corresponding capacity retentions are 1.4%, 30.9%, 32.3%, 41.3%, and 37.0% in sequence. Obviously, the coated samples exhibit better cycle performance than sample 0, and sample 3 shows the highest capacity retention. So a moderate amount of Li_3VO_4 can improve the cycle stability of $Li[Ni_{0.5}Co_{0.2}Mn_{0.3}]O_2$ at higher discharge rate.

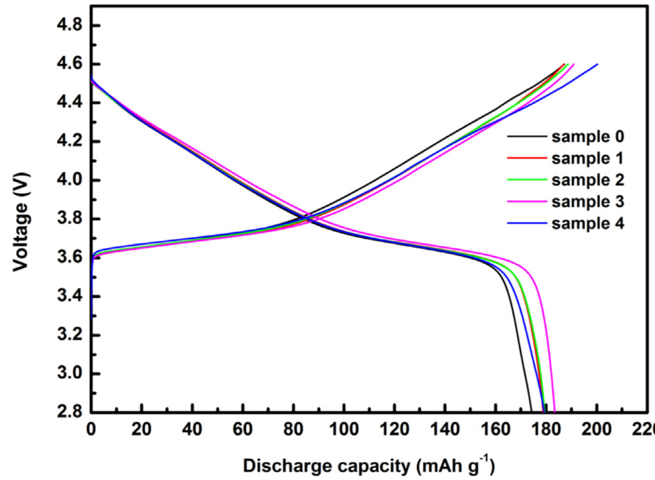

Fig. 1. Initial charge–discharge curves of samples at 0.1 C between 2.8 and 4.6 V.

XPS wide-spectra of sample 0 and sample 3 are given in Fig. 3, and the O1s and Li1s spectra are shown in Fig. 4. In Fig. 3, the V2p peak at 517.19 eV, which is characteristic of V^{5+} in Li_3VO_4 [15,16], is presented in sample 3. Moreover, the higher atom ratio of O1s to M2p (Mn2p, Co2p, and Ni2p) in sample 3 suggests a stronger oxygen adsorption ability [17] on sample 3 surface. The results prove that the V–O bond has formed on $Li[Ni_{0.5}Co_{0.2}Mn_{0.3}]O_2$ surface, and directly indicate that $Li[Ni_{0.5}Co_{0.2}Mn_{0.3}]O_2$ has been successfully coated with Li_3VO_4.

The XPS spectra of O1s and Li1s have been obviously changed by Li_3VO_4 coating layer. For sample 0 (in Fig. 4a–b), the O1s peak at 529.03 eV and Li1s peak at 53.88 eV can be attributed to the signal of oxygen and lithium in the $Li[Ni_{0.5}Co_{0.2}Mn_{0.3}]O_2$ crystalline network [18,19], while the O1s peak at 531.10 eV and Li1s peak at 54.85 eV can be assigned to the surface impurities (Li_2CO_3, LiOH, etc.) [20]. After coating, the peak area ratios of O1s (at 531.31 eV) and Li1s (at 55.05 eV) in Fig. 4c–d become lager than that of O1s (at 531.10 eV) and Li1s (at 54.85 eV), respectively, in Fig. 4a–b, which indicates there exists much more oxygen and lithium on sample 3 surface due to the presence of Li_3VO_4. In addition, the couple peaks of O1s for sample 3 shift by 0.21–0.37 eV toward the higher binding energies which indirectly implies that Li_3VO_4 might be adhered

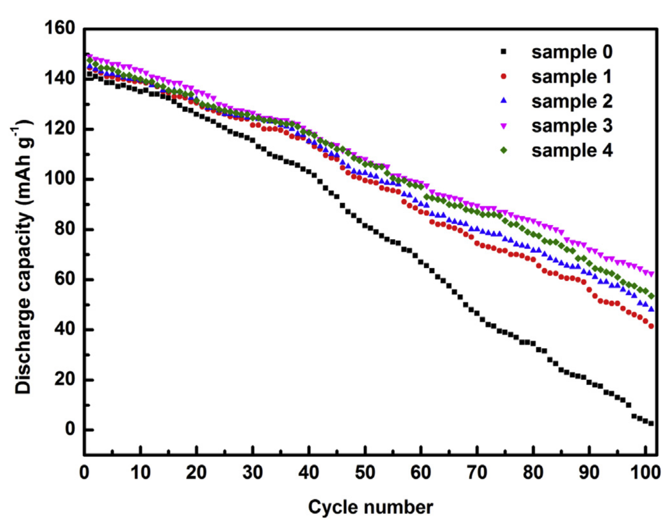

Fig. 2. Cycle performance of samples at 10 C between 2.8 and 4.6 V after 100 cycles.

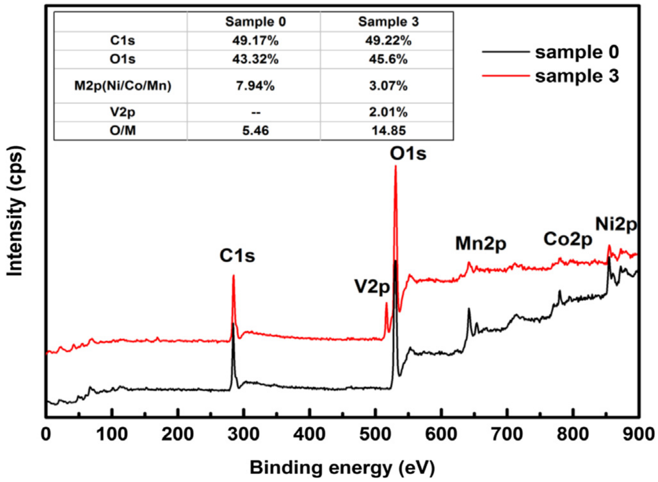

Fig. 3. XPS wide-scan spectra of sample 0 and sample 3.

strongly on Li$[Ni_{0.5}Co_{0.2}Mn_{0.3}]O_2$ surface. Thus, we infer that the chemical interaction [21,22] between Li$[Ni_{0.5}Co_{0.2}Mn_{0.3}]O_2$ and Li_3VO_4 leads to the formation of a stable protective layer on Li$[Ni_{0.5}Co_{0.2}Mn_{0.3}]O_2$ surface.

Rate capabilities of sample 0 and sample 3 are further investigated in Fig. 5. After activated at 0.05 C (9 mA g^{-1}) rate, the cells are charged to 4.6 V at 0.1 C (18 mA g^{-1}), and discharged to 2.8 V at 0.5 C (90 mA g^{-1}), 1 C, 2 C, 5 C, 10 C, and 20 C rate, respectively, then cycled at 0.5 C again. Sample 3 obviously exhibits a much better rate capability at any rates, especially at high rates 5 C and 10 C. Li_3VO_4, whose ionic conductivity has been reported to be $\sim 4 \times 10^{-5}$ S cm^{-1} [23], is identified as a Li-ion conductor [24], so the result indicates the Li_3VO_4 coating layer can obviously improve Li^+ conductivity of Li$[Ni_{0.5}Co_{0.2}Mn_{0.3}]O_2$. And sample 3 can still retain 80.0% of its initial capacity (118.0 mAh g^{-1}) at 20 C discharge rate, while sample 0 only sustains 109.1 mAh g^{-1} at the same rate. When cycled at 0.5 C again, the capacity coverage of sample 3 (92.4%) is higher than that of sample 0 (90.8%), so the Li_3VO_4 layer helps to retard the capacity fading at high current density.

The cycliability of sample 0 and sample 3 at 1 C under different cut-off voltages (4.6 V and 4.8 V) are further compared in Fig. 6. At both cut-off voltages, sample 3 delivers higher discharge capacity than sample 0. The capacity retention of sample 0 after 100 cycles drops obviously from 51.2% (4.6 V) to 41.5% (4.8 V), but that of sample 3 has only a slight drop from 63.5% (4.6 V) to 63.0% (4.8 V), indicating that Li_3VO_4 coating helps to attain a high energy density. The better capacity retentions of sample 3 at both voltages indicate its obviously improved high voltage cycling behavior. What's more, the capacity retention of sample 3 decreases slightly with increasing the voltage. Therefore, the improved cycliability of Li$[Ni_{0.5}Co_{0.2}Mn_{0.3}]O_2$ at high voltage region can be obtained by Li_3VO_4 coating.

Fig. 7 shows the CV curves of sample 0 and sample 3 for the first three cycles and the 50th cycle. In Fig. 7a, the anodic/cathodic peaks of Ni^{2+}/Ni^{4+} [12] and Co^{3+}/Co^{4+} [14] couples in the first cycle, respectively, appear at 3.85 V/3.70 V and 4.40 V/4.31 V. In the subsequent two cycles, the relative intensity of major redox peaks

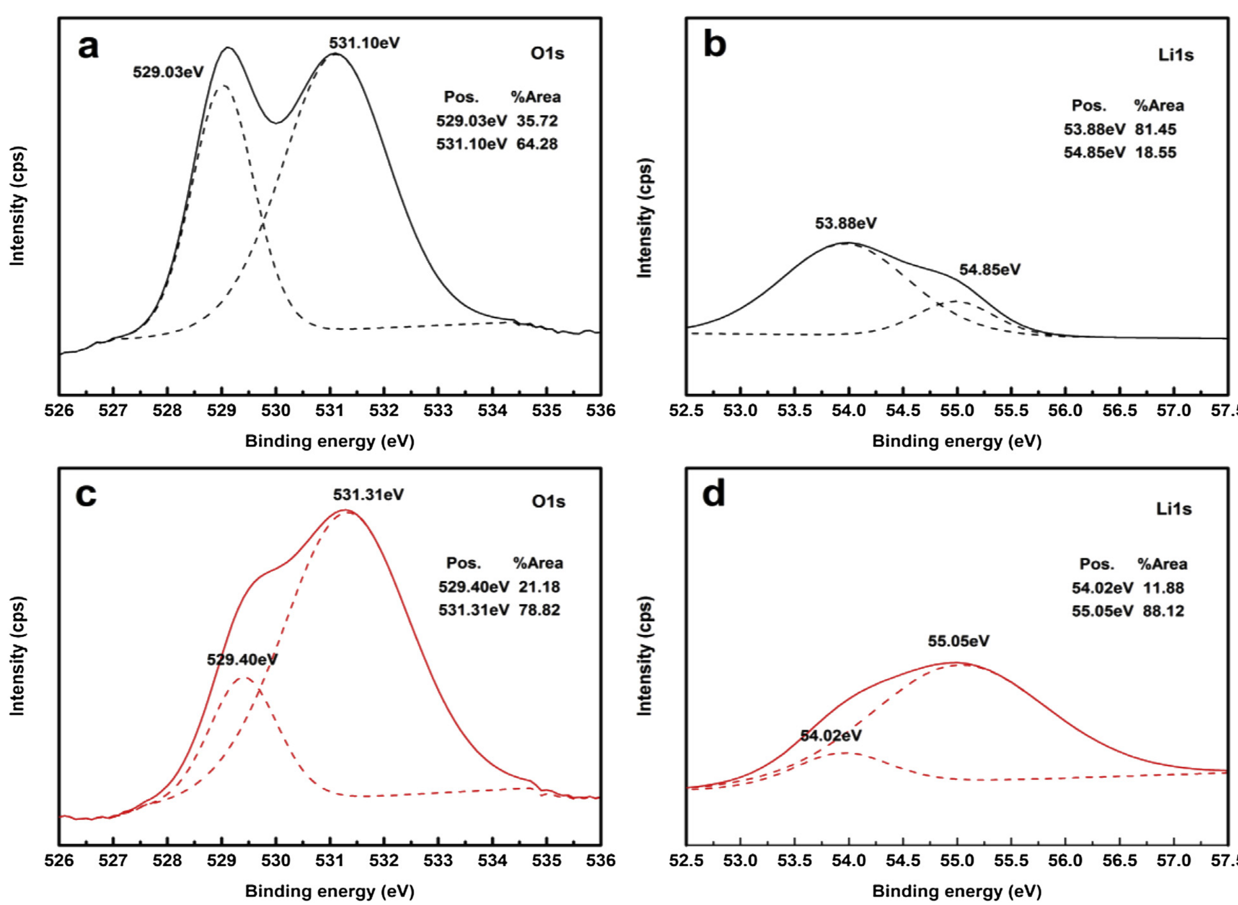

Fig. 4. XPS spectra of O1s and Li1s for a–b) sample 0 and c–d) sample 3.

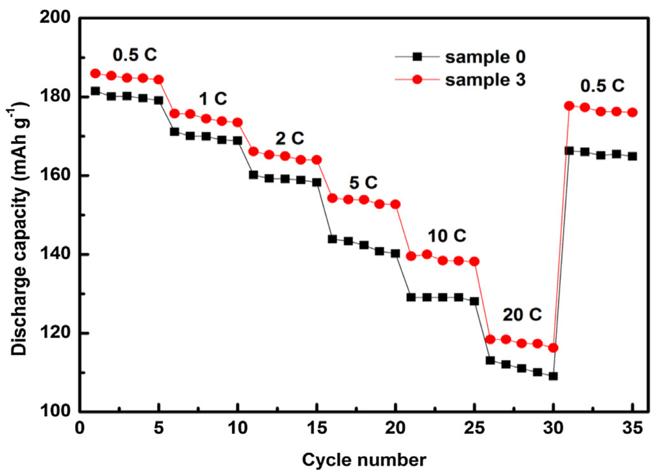

Fig. 5. Discharge rate capability at different rates between 2.8 and 4.6 V.

and the peak separation (AEp) between anodic peak and cathodic peak both decrease, so the irreversible loss of lithium [25] and the polarization degree [26] are reduced. It should also be noted that a weak and broad oxidation peak corresponding to Co and Mn dissolution [27,28] appears at 4.75 V in sample 0 when the potential scan is expanded to 4.9 V. After 50 cycles at 1 C, the major redox peaks become broader and the AEp increases to 360 mV, which indicates larger irreversible degree of the electrode reaction. What's more, a broadened anodic peak appears in the range of 4.25–4.80 V, which indicates that some side reactions occur at electrode/electrolyte interface with cycling.

Except for the peaks of Ni^{2+}/Ni^{4+} and Co^{3+}/Co^{4+} couples, no redundant redox peaks can be observed for sample 3 in Fig. 7b, which suggests that Li_3VO_4 layer is not involved in the electrode reaction, and the dissolution of Co and Mn ions on high voltage region has been suppressed. After 50 cycles, the distinct anodic/cathodic peaks of Ni^{2+}/Ni^{4+} couple for sample 3 have unobvious change, but a smaller AEp value (301 mV) is observed. So the CV results suggest that sample 3 shows higher structural stability and reversibility degree by suppressing the dissolution [29] of Li$[Ni_{0.5}Co_{0.2}Mn_{0.3}]O_2$, which is consistent with the result of the cycle performance studies well.

Fig. 8 presents the Nyquist plots of sample 0 and sample 3 at 10 C between 2.8 V and 4.6 V (before and after 50 and 100 cycles). The curves are all composed of a high-to-medium frequency semicircle and a straight line at low frequency which, respectively, correspond to interfacial charge transfer resistance (R_{ct}) and Li^+ diffusion coefficient (D_{Li+}) [30]. R_{ct} is obtained by fitting ZSimpWin software. In addition, D_{Li+} is calculated using the following equations [31,32]:

$$D_{Li^+} = \frac{R^2T^2}{2A^2n^4F^4c^2\sigma^2}$$

where A denotes the surface area of the electrode, n is the number of shifted electrons, F is the Faraday constant, c is the concentration of Li^+, and σ is the Warburg factor. R_{ct} values and D_{Li+} values are listed in Table 1. Before cycling, sample 3 exhibits a lower R_{ct} (100.2 Ω) than sample 0 (149.6 Ω), and a higher D_{Li+} (1.77×10^{-11} cm^2 s^{-1}) than sample 0 (8.8×10^{-12} cm^2 s^{-1}) and the related report (1.70×10^{-11} cm^2 s^{-1} [14]). With cycling, the R_{ct} values of sample 3 increases much less than that of sample 0, concurrently its D_{Li+} decreases obviously less than that of sample 0. The above results imply that the Li_3VO_4 layer can not only enhance the Li^+ transport rate in Li$[Ni_{0.5}Co_{0.2}Mn_{0.3}]O_2$ material, but also decrease the electrode polarization during repeated Li^+ insertion/extraction.

In order to study the intrinsic reason for performance improvement, sample 0 and sample 3 before and after the 50th cycle at 10 C between 2.8 and 4.6 V were characterized by XRD, respectively. The XRD patterns of are shown in Fig. 9. The patterns of uncycled sample 0 and sample 3 can be well indexed to hexagonal α-$NaFeO_2$ structure with a $R\overline{3}m$ space group. Both the sharp diffraction peaks and the clear splits of (006)/(102) and (108)/(110) doublets indicate the formation of a well-ordered layer structure [9]. But some weak peaks of Li_3VO_4 phase appear between 21° and 25° for uncycled sample 3 in the inset of Fig. 9, which are assigned to orthorhombic structure with a Pnm21 space group [33,23]. After the 50th cycle, the diffraction peaks of sample 0 shift to a higher angle which indicates its structure changes during cycling, while the peaks of sample 3 have no obvious shift except the Li_3VO_4 peaks disappear. The absence of Li_3VO_4 peak is attributed to the decrease of the coating amount of Li_3VO_4 on Li$[Ni_{0.5}Co_{0.2}Mn_{0.3}]O_2$ surface which is too little to be detected [34].

The lattice parameters calculated from the refined XRD patterns are shown in Table 2. Before cycling, the identical lattice parameters of sample 0 and sample 3 suggest no vanadium element is doped into the Li$[Ni_{0.5}Co_{0.2}Mn_{0.3}]O_2$ lattice. After the 50th cycle, *a*

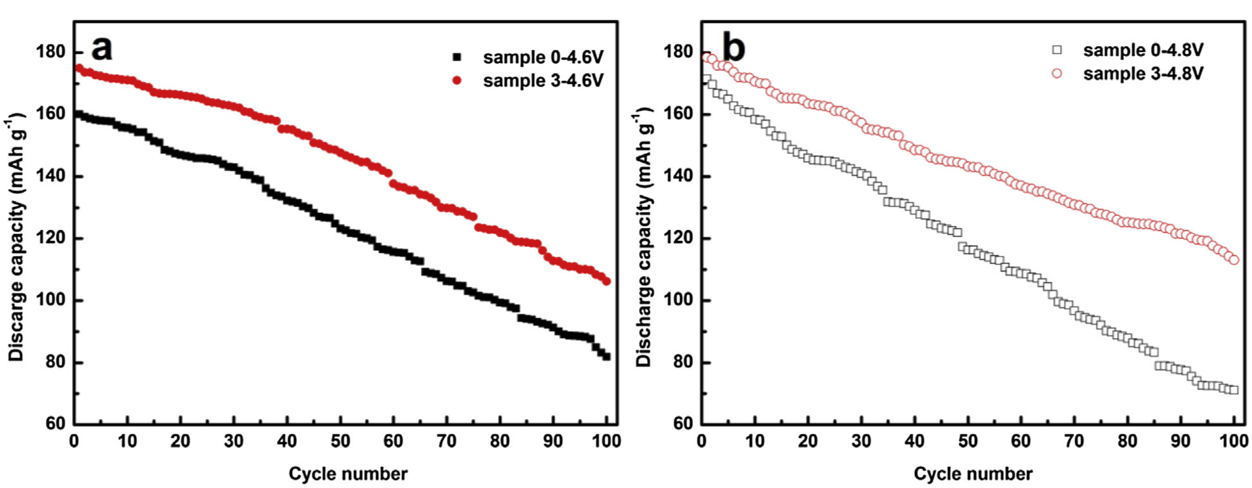

Fig. 6. Cycle performances of sample 0 and sample 3 at 1 C in the voltage range of a) 2.8–4.6 V and b) 2.8–4.8 V.

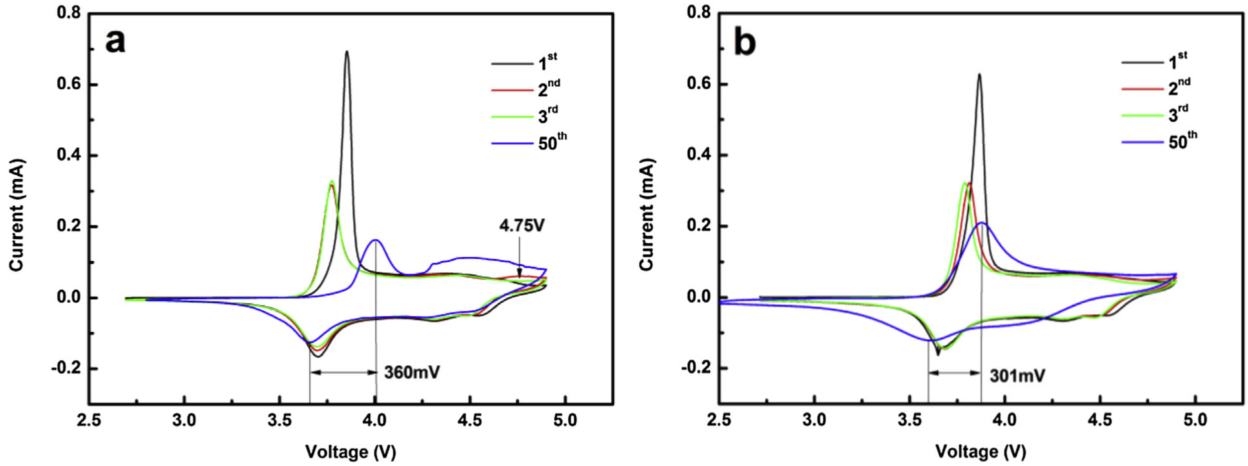

Fig. 7. CV curves between 2.5 and 4.9 V with a scan rate of 0.05 mv s^{-1} of a) sample 0 and b) sample 3.

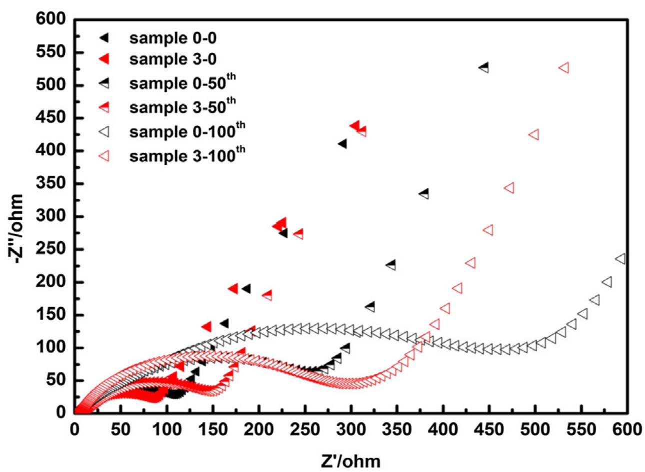

Fig. 8. Nyquist plots of sample 0 and sample 3.

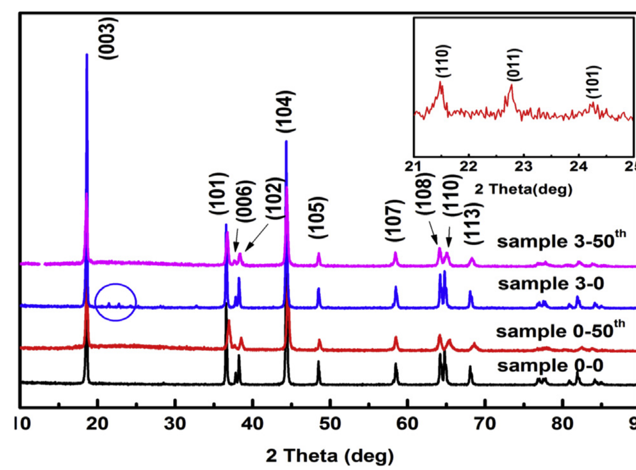

Fig. 9. XRD patterns of sample 0 and sample 3 before and after 50 cycles at 10 C between 2.8 and 4.6 V.

(interatomic distance) decreases and *c* (interplanar distance) increases concurrently. The shrinkage of a means irreversible extraction of Li^+, and the increase of *c* means the electrostatic repulsion by the irreversible removal of Li^+ [35]. Both the *a*, *c* changes and unit-cell volume shrinkage for sample 0 are larger than that for sample 3, which indicate the Li^+ diffusion tunnels for sample 0 have been seriously destroyed [36] after cycling. Because the changes of unit-cell parameters are related to the change of crystal structure, Li_3VO_4 layer plays an important role in alleviating structural damage of $Li[Ni_{0.5}Co_{0.2}Mn_{0.3}]O_2$.

The TEM images accompanied by EDS spectra of sample 3 before cycling and after 50 cycles at 10 C between 2.8 and 4.6 V are shown in Fig. 10. Before cycling, the TEM images in Fig. 10a show that Li_3VO_4 nanocrystals are coated on the $Li[Ni_{0.5}Co_{0.2}Mn_{0.3}]O_2$ surface, and EDS in Fig. 10c confirms the existence of V component in coating layer. Fig. 10b, the local enlarged images of Fig. 10a, clearly exhibits a Li_3VO_4 coating layer. Furthermore, the clear lattice fringes in the inset of Fig. 10b indicate the highly crystalline nature of Li_3VO_4 particle which has been confirmed by XRD.

After cycling, some Li_3VO_4 nanoparticles still can be observed on $Li[Ni_{0.5}Co_{0.2}Mn_{0.3}]O_2$ surface in Fig. 10d, but the coating layer in Fig. 10e becomes loose and untight compared with that of uncycled sample in Fig. 10b. We contribute it to the gradual pulverization of Li_3VO_4 particles, which makes the electric-contact between particles worse and finally results in the slow capacity fading [37]. The inset in Fig. 10e illustrates the clear lattice fringes of Li_3VO_4, which

Table 1
Fitting results for impedance spectra and calculated D_{Li+}.

Sample	Cycles	R_{ct}/Ω	$D_{Li+}/cm^2\ s^{-1}$
Sample 0	0	149.6	8.8×10^{-12}
	50th	294.1	1.36×10^{-12}
	100th	446.2	4.17×10^{-12}
Sample 3	0	100.2	1.77×10^{-11}
	50th	205.1	8.95×10^{-12}
	100th	329.4	6.68×10^{-12}

Table 2
Calculated structure parameters of sample 0 and sample 3.

Samples	Cycles	a/Å	c/Å	c/a	V/Å^{-3}
Sample 0	0	2.876	14.260	4.958	102.1
	50th	2.850	14.332	5.029	100.8
Sample 3	0	2.876	14.260	4.958	102.1
	50th	2.872	14.270	4.969	102.0

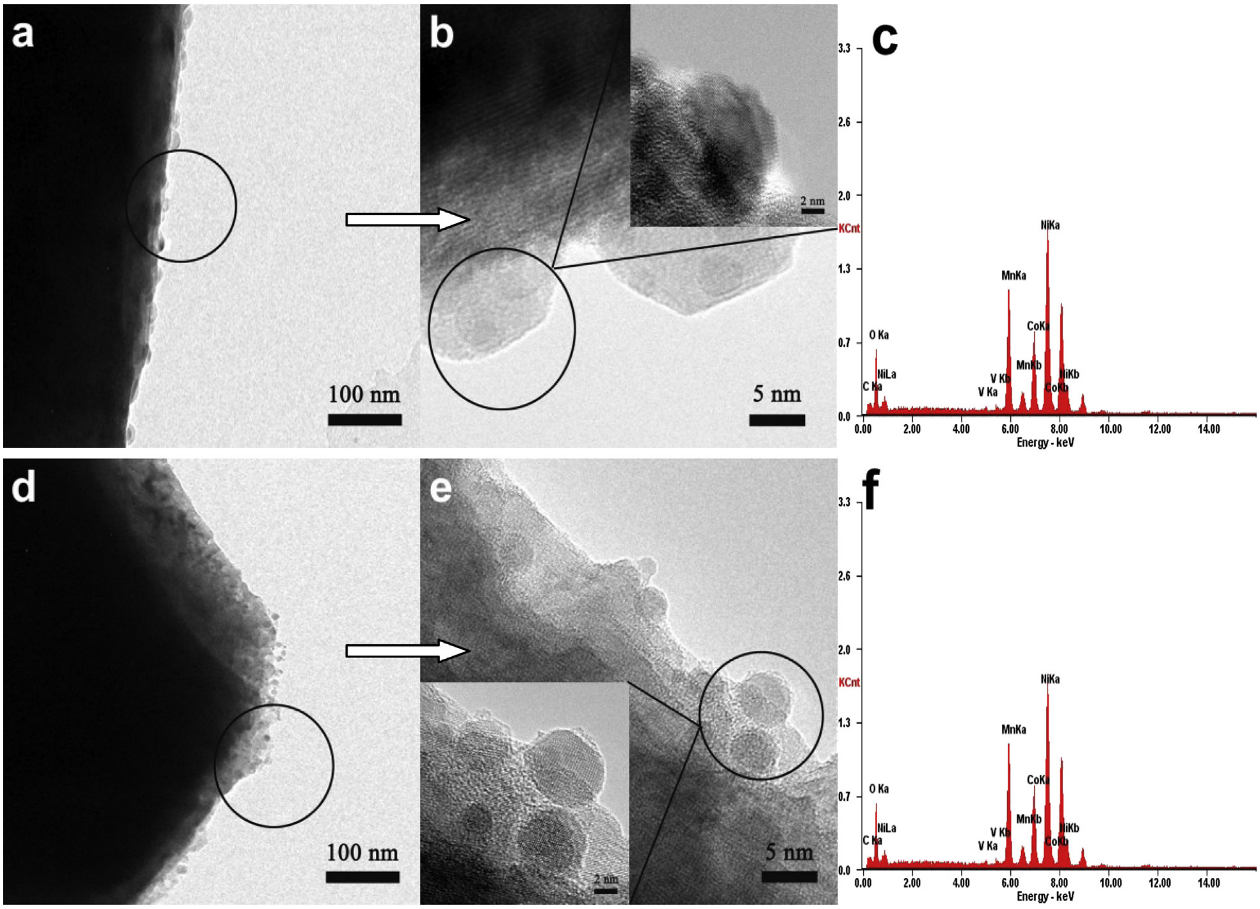

Fig. 10. TEM images and corresponding EDS spectra of sample 3 a–c) before cycling and d–f) after 50 cycles at 10 C between 2.8 and 4.6 V.

implies the structure of Li_3VO_4 is relatively stable during repeated charge/discharge processes.

4. Conclusion

Li_3VO_4 surface modification plays an effective role in improving the electrochemical performances of $Li[Ni_{0.5}Co_{0.2}Mn_{0.3}]O_2$ cathode material, especially the cycle stability at high discharge rate or high voltage region. $Li[Ni_{0.5}Co_{0.2}Mn_{0.3}]O_2$ coated with 3 wt.% Li_3VO_4 (sample 3), respectively, exhibits the highest capacity retention of 63.5% and 63.0% under different cut-off voltages 4.6 V and 4.8 V at 1 C. Sample 3 also gives the best high-rate performance, which can retain 118.0 mAh g^{-1} at 20 C rate. The improved electrochemical performances can be attributed to decreased polarization, enhanced Li^+ conductivity, and higher structure stability of $Li[Ni_{0.5}Co_{0.2}Mn_{0.3}]O_2$ by protective Li_3VO_4 layer which can restrain the side reactions at electrode/electrolyte interface and the dissolution of $Li[Ni_{0.5}Co_{0.2}Mn_{0.3}]O_2$ during cycling, even at high cut-off voltage 4.8 V.

Acknowledgment

The authors acknowledge the financial support of Tianjin Huaxia Hongyuan Industrial Co., Ltd.

References

[1] Y. Cho, P. Oh, J. Cho, Nano Lett. 13 (2013) 1145–1152.
[2] Z.L. Liu, A.S. Yu, J.Y. Lee, J. Power Sources 81-82 (1999) 416–419.
[3] Y. Shao-Horn, L. Croguennec, C. Delmas, E.C. Nelson, M.A. O'Keefe, Nat. Mater. 2 (2003) 464–467.
[4] H.-S. Kim, M.Z. Kong, K. Kim, I.-J. Kim, H.-B. Gu, J. Power Sources 171 (2007) 917–921.
[5] W.-S. Kim, S.-B. Kim, I.C. Jang, H.H. Lim, Y.S. Lee, J. Alloys Compd. 492 (2010) L87–L90.
[6] X.X. Zuo, C.J. Fan, J.S. Liu, X. Xiao, J.H. Wu, J.M. Nan, J. Power Sources 229 (2013) 308–312.
[7] N.V. Kosova, E.T. Devyatkina, V.V. Kaichev, J. Power Sources 174 (2007) 965–969.
[8] L. Croguennec, J. Bains, J. Bréger, C. Tessier, Ph. Biensan, S. Levasseur, C. Delmas, J. Electrochem. Soc. 158 (2011) A664–A670.
[9] D. Wang, Y. Huang, Z.Q. Huo, L. Chen, Electrochim. Acta 107 (2013) 461–466.
[10] S. Sivaprakash, S.B. Majumder, J. Alloys Compd. 479 (2009) 561–568.
[11] G.T.K. Fey, J.G. Chen, V. Subramanian, T. Osaka, J. Power Sources 112 (2002) 384–394.
[12] X.Z. Liu, P. He, H.Q. Li, M. Ishida, H.S. Zhou, J. Alloys Compd. 552 (2013) 76–82.
[13] X. Pu, C. Yu, Nanoscale 4 (2012) 6743–6747.
[14] S.Y. Yang, X.Y. Wang, X.K. Yang, Y.S. Bai, Z.L. Liu, H.B. Shu, Q.L. Wei, Electrochim. Acta 66 (2012) 88–93.
[15] J. Światowska-Mrowiecka, V. Maurice, S. Zanna, L. Klein, P. Marcus, Electrochim. Acta 52 (2007) 5644–5653.
[16] H. Yu, X.H. Rui, H.T. Tan, J. Chen, X. Huang, C. Xu, W.L. Liu, D.Y.W. Yu, H.H. Hng, H.E. Hoster, Q.Y. Yan, Nanoscale 5 (2013) 4937–4943.
[17] C.H. Zhang, L. Fu, N. Liu, M.H. Liu, Y.Y. Wang, Z.F. Liu, Adv. Mater. 23 (2011) 1020–1024.
[18] W. Liu, M. Wang, X.L. Gao, W.D. Zhang, J.T. Chen, H.H. Zhou, X.X. Zhang, J. Alloys Compd. 543 (2012) 181–188.
[19] Y. Wu, A.V. Murugan, A. Manthiram, J. Electrochem. Soc. 155 (2008) A635–A641.
[20] K. Kanamura, S. Shiraishi, H. Tamura, Z.-I. Takehara, J. Electrochem. Soc. 141 (1994) 2379–2385.
[21] Y. Zubavichus, M. Zharnikov, Y.J. Yang, O. Fuchs, C. Heske, E. Umbach, G. Tzvetkov, F.P. Netzer, M. Grunze, J. Phys. Chem. B 109 (2005) 884–891.
[22] R. Cueff, G. Baud, M. Benmalek, J.P. Besse, J.R. Butruille, M. Jacquet, Appl. Surf. Sci. 115 (1997) 292–298.
[23] H.Q. Li, X.Z. Liu, T.Y. Zhai, D. Li, H.S. Zhou, Adv. Energy Mater. 3 (2013) 428–432.

[24] X. Pu, L. Yin, C. Yu, J. Nanopart. Res. 14 (2012) 1–7.
[25] J.-H. Ju, K.-S. Ryu, J. Alloys Compd. 509 (2011) 7985–7992.
[26] T. Liu, S.-X. Zhao, K.Z. Wang, C.-W. Nan, Electrochim. Acta 85 (2012) 605–611.
[27] H.H. Zheng, Q.N. Sun, G. Liu, X.Y. Song, V.S. Battaglia, J. Power Sources 207 (2012) 134–140.
[28] K. Yang, L.-Z. Fan, J. Guo, X.H. Qu, Electrochim. Acta 63 (2012) 363–368.
[29] A.M. Kannan, L. Rabenberg, A. Manthiram, Electrochem. Solid-State Lett. 6 (2003) A16–A18.
[30] S.S. Zhang, K. Xu, T.R. Jow, Electrochim. Acta 49 (2004) 1057–1061.
[31] K. Kim, S.H. Park, T.H. Kwon, J.E. Park, H. Ahn, M.-J. Lee, Electrochim. Acta 89 (2013) 708–716.
[32] Z.-Q. Huo, Y.-T. Cui, D. Wang, Y. Dong, L. Chen, J. Power Sources 245 (2014) 331–336.
[33] W.-T. Kim, Y.U. Jeong, Y.J. Lee, Y.J. Kim, J.H. Song, J. Power Sources 244 (2013) 557–560.
[34] Z.Y. Wang, E.Z. Liu, C.N. He, C.S. Shi, J.J. Li, N.Q. Zhao, J. Power Sources 236 (2013) 25–32.
[35] Y.W. Tsai, B.J. Hwang, G. Ceder, H.S. Sheu, D.G. Liu, J.F. Lee, Chem. Mater. 17 (2005) 3191–3199.
[36] L.A. Montoro, J.M. Rosolen, Electrochim. Acta 49 (2004) 3243–3249.
[37] X.F. Li, X.B. Meng, J. Liu, D.S. Geng, Y. Zhang, M.N. Banis, Y.L. Li, J.L. Yang, R.Y. Li, X.L. Sun, M. Cai, M.W. Verbrugge, Adv. Funct. Mater. 22 (2012) 1647–1654.